I&EC research
Industrial & Engineering Chemistry Research

Article

pubs.acs.org/IECR

Granular Flow in Silo Discharge: Discrete Element Method Simulations and Model Assessment

V. Vidyapati[†] and S. Subramaniam*

Department of Mechanical Engineering, Center for Computational Thermal-Fluids Research, Iowa State University, Ames, Iowa 50011, United States

ABSTRACT: Discharge dynamics of granular particles from a flat-bottomed silo is studied using both continuum modeling and three-dimensional (3D) discrete element method (DEM) simulations. Using DEM, the influence of microscopic parameters (interparticle friction coefficient, particle−wall friction coefficient and particle coefficient of restitution) and system parameters (orifice width) on the discharge rate is quantified. The spatial extent of different regimes (quasi-static, intermediate and inertial) of granular rheology are quantified using a regime map previously established from DEM data of homogeneously sheared granular flow. It is shown that all three regimes of granular rheology coexist during silo discharge, and the intermediate regime plays a significant role in discharge dynamics. A quantitative comparison between results of continuum and DEM simulations is performed by computing discharge rates, solid velocities, and solid stresses for a three-dimensional (3D) flat-bottomed silo. It is found that the three constitutive models investigated in this study overpredict the discharge rate when compared to DEM data. Contour plots of the error in solid stress prediction are compared with the spatial extent of different regimes of granular rheology to deduce that it is inaccurate modeling of the intermediate regime that is responsible for overprediction of the discharge rate.

1. INTRODUCTION

Modeling and prediction of granular flows in nature and in technological applications is a challenging problem of considerable socioeconomic importance.[1] For example, solids processing is a multibillion dollar industry that is a critical part of the pharmaceutical (e.g., capsule, tablet solids), agricultural (e.g., fruits, seed processing), and consumer product (e.g., cereal, detergent, canned goods) industries. Silos are one of the important devices widely used in the processing and handling of granular materials in many industrial and agricultural applications.[2] Accurate prediction of the discharge rate is critical for dependable design and optimum performance of these devices. There are two different numerical approaches that are commonly used to study discharge dynamics of a silo. The first approach, DEM (discrete element method), is a particle-level microscopic simulation method that represents multiparticle interaction on contact through a contact force model.[3] The computational cost of DEM restricts its use to relatively small system sizes and idealized geometries. The second approach is a continuum description of granular flows that results in averaged conservation equations for mass, momentum, and energy. The continuum approach is used for simulations of device-scale granular flows because the cost of simulating individual particles is prohibitive for large systems.

In the continuum approach, the granular stress needs to be modeled using a constitutive relation that should correctly reflect the rheological behavior of granular flow as a function of macroscopic conditions (shear rate and solid volume fraction) and microscopic properties (e.g., interparticle friction and coefficient of restitution). Granular rheology is complex, with the existence of at least three distinct regimes (quasi-static, intermediate, and inertial) emerging from experiments[4] and DEM simulations.[5−8] Constitutive models for the inertial (rapid flow) regime have been successfully developed by means of corrections to the kinetic theory of gases,[9−11] whereas the quasi-static regime is generally described by plasticity theories.[12−14] However, no unified theory has been proposed for the intermediate (transitional) flow regime,[4,15,16] where both collisional and frictional interactions between particles are important.

Benyahia[17] performed validation studies of different constitutive models for granular flow in the frictional regime by comparing discharge rates from a two-dimensional (2D) bin with the Beverloo correlation[18] $[\dot{m} = 0.58\rho_b g^{0.5}(D - kd_p)^{2.5}]$ for different orifice widths. The first constitutive model assessed in his work[17] is the model proposed by Schaeffer,[12] which has been traditionally used in the MFIX computer code.[19] The second model he assessed is the constitutive model developed by Srivastava and Sundaresan,[20] referred to as the S&S model for brevity. Srivastava and Sundaresan[20] conducted a validation study of their model by comparing discharge rate with the well−known Beverloo correlation[18] for a 2D bin. These studies[17,20] found that the discharge rate predicted by existing continuum theories does not match well with that obtained from the Beverloo correlation[18] of experimental data.

We also confirm this observation by performing continuum simulations of the same 2D bin discharge problem that was earlier studied by Srivastava and Sundaresan[20] and Benyahia.[17] Figure 1a shows the temporal variation of the discharge rate obtained from two different constitutive models (the Schaeffer model[12] and S&S model[20]) compared with the Beverloo correlation[18] of experimental data. This result shows that both constitutive models predict discharge rates that are much higher (more than 70%) than that obtained using the Beverloo

Received: December 26, 2012
Revised: August 10, 2013
Accepted: August 15, 2013
Published: August 15, 2013

dx.doi.org/10.1021/ie303598e | *Ind. Eng. Chem. Res.* 2013, 52, 13171−13182

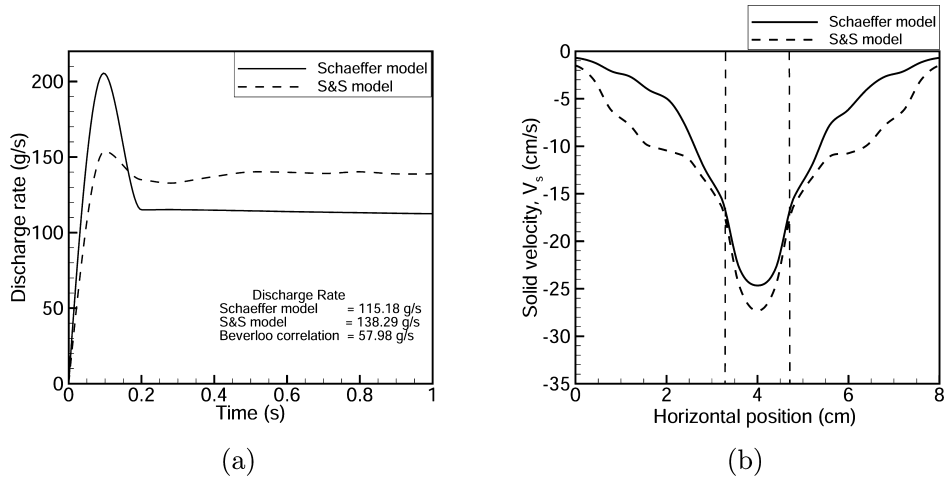

Figure 1. (a) Temporal variation of discharge rate using two different continuum models and (b) transverse solid velocity profile during steady discharge at time t = 4.0 s, at 1 cm above the discharge orifice. The dashed vertical lines indicate the location of the edge of the orifice.

correlation[18] [$\dot{m} = 0.58\rho_b g^{0.5}(D - kd_p)^{2.5}$]. Figure 1b shows the profile of transverse solid velocity during steady discharge at time t = 4.0 s, at 1 cm above the discharge orifice. This figure reveals that both constitutive models predict that there is some flow even in the corners of the bin, whereas these regions should really be stagnant, as previously observed in experiments.[21] One reason for this discrepancy in the prediction of the discharge rate and the discharge velocity is that not all particle−particle interactions are correctly represented or modeled in the continuum simulations.

This motivates our use of DEM simulations, which represent important particle−particle interactions, as a route to understanding the deficiencies in the continuum simulations and for suggesting improvements. Although restricted to relatively small system sizes and idealized geometries, DEM simulations can be used to evaluate and develop improved constitutive models for particulate flows. The rapid increase of computing power and advances in numerical methods have made it possible to perform detailed and accurate DEM simulations of particulate flows. Several studies have been performed to understand the discharge dynamics of granular particles from silos and hoppers[22−24] using DEM. Landry et al.[22] studied the vertical stress profile in two- and three-dimensional (3D) silos and further examined how this stress profile changes with dimensionality. Their analysis revealed that the Janssen theory does not fully describe these packings, especially at the top of the piles. They also found a number of noticeable differences between 2D and 3D packings. For instance, their study shows that 2D packings support much less vertical stress than 3D packings. Most DEM simulations of silo discharge thus far have been confined to 2D systems. Hence, the work of Landry et al.[22] motivates the need for 3D DEM simulations of silo discharge.

Goda and Ebert[23] performed a detailed DEM study on a 3D silo. However, their study was limited to studying the distribution of normal wall forces and pressure developed at the end of the filling process. Ketterhagen et al.[24] performed a systematic study to quantify the modes of powder flow in a series of 3D conical hoppers and quasi-3D wedge-shaped hoppers using DEM simulations. These flow modes (mass flow or funnel flow) are quantified using a mass flow index (MFI), which is defined as the ratio of the mean particle velocity at the hopper wall to the mean particle velocity at the hopper centerline. The existence of these different flow modes can be directly related to different levels of shear stress at the silo wall. Further, as we show later in this work, these different levels of shear stress could be the result of the coexistence of different regimes (quasi-static, intermediate, and inertial) of granular rheology, which we quantify using DEM simulations.

As noted previously, granular rheology is a function of both macroscopic conditions and microscopic properties. Experiments[25] and DEM simulations[5,7,8,26] have shown that microscopic properties such as the interparticle friction coefficient can significantly affect the rheology of granular flows. For example, Engblom et al.[25] performed experiments to study the segregation mechanics of powder mixtures in a cylindrical silo due to variation in material properties. They found that material properties (such as interparticle friction) have a significant effect on the distribution of powder mixing. This result indicates the need for more precise quantification of the effect of material properties (such as the particle friction coefficient and the coefficient of restitution) on the different regimes of granular rheology, and on the silo discharge rate. Note that Beverloo's correlation of experimental data that is widely used to calculate the discharge rate[18] does not include the effect of particle friction. Anand et al.[27] studied the discharge from a 3D rectangular hopper using DEM and quantified the effect of different simulation parameters (such as interparticle friction coefficient, particle−wall friction coefficient, orifice width, and particle coefficient of restitution) on the discharge rate. However, we are not aware of a comprehensive study that compares results of DEM and continuum simulations for a 3D silo.

In this work, a 3D flat-bottomed silo is simulated using DEM, and the effect of different microscopic (interparticle friction coefficient, particle−wall friction coefficient, and coefficient of restitution) and system parameters (discharge outlet size) on the discharge rate is studied. Further, we quantify the spatial extent of different regimes (inertial, intermediate, and quasi-static) of granular rheology in this silo discharge problem using a comprehensive regime map[26] that was previously established using 3D DEM data of homogeneously sheared granular flow. The effect of interparticle friction coefficient on the spatial extent of these different regimes of granular rheology is also studied. A direct quantitative comparison between DEM and

continuum simulation is performed by comparing the outlet solid velocity profile and solid stresses inside the silo.

The next section discusses the DEM simulations of silo discharge along with a description of the method used to characterize the spatial extent of different regimes of granular rheology in the silo discharge problem. The following section describes the details of 3D continuum simulations, including a brief description of three different constitutive models that are assessed in this work. In section 3.3 we discuss results from a quantitative comparison between DEM and continuum simulations for a 3D flat-bottomed silo. Finally, conclusions are drawn in section 4.

2. DISCRETE ELEMENT METHOD SIMULATIONS

In order to infer local flow behavior and to have a direct quantitative comparison with continuum simulations, we perform 3D DEM simulations of silo discharge. The DEM simulations model the granular material as a particle assembly consisting of monodisperse, spherical, cohesionless particles of diameter d_p and mass m_p. A soft sphere model is used, in which particles interact via contact laws and friction only on contact. Since the realistic modeling of particle deformation is complicated, a simplified contact force model based on a linear spring−dashpot combination is used in this work.[3] Details of the computational model used in these discrete element simulations are given in the Appendix. For all the DEM simulations reported, the mass and diameter of particles are set to 1, so the density of particles is $6/\pi$. The value of normal spring constant (k_n) is set to 2×10^5 ($m_p g/d_p$ units), which captures the general behavior of intermediate to high k_n systems.[3] The integration time step Δt for all the DEM simulations is selected to be $t_c/50$, where t_c is the binary collision time. This time step is shown to be sufficiently small to ensure temporal convergence.[3]

2.1. DEM Simulations of Silo Discharge. The movement of individual particles during the outflow caused by gravity is studied using 3D DEM simulations. The domain size selected for these simulations is $18 \times 18 \times 36$ particle diameter units in the x, y, and z directions, respectively. It is shown later in this section that this system size is big enough to ensure a discharge rate that is independent of domain size. The only external force acting on the system is gravity in the negative z direction. In all these DEM simulations the discharge outlet is circular in shape with diameter $6d_p$, where d_p is the particle diameter (except for a few simulations that are performed to quantify the effect of discharge outlet size on the discharge rate). The domain is bounded by flat−frictional walls in all the directions (x, y, and z). The number of particles simulated in this study varies between 11 136 and 13 340, depending on the initial solid volume fraction and domain size for a specific simulation.

To ensure a constant discharge rate that is independent of domain size, the following design constraints are used:[27]

(1) $D \geq 6d_p$, where D is the size of discharge outlet and d_p is the particle diameter.
(2) $H > D$, where H is the fill height at centerline.
(3) $W > 2.5D$, where W is the silo width.

In order to ensure that the discharge rate from the silo remains unchanged with domain size, we performed DEM simulations with different domain sizes. Figure 2 shows the amount of mass discharged with time for a simulation with initial solid volume fraction of 0.60, for four different domain sizes of $12d_p \times 12d_p \times 24d_p$, $15d_p \times 15d_p \times 30d_p$, $16d_p \times 16d_p \times 30d_p$, and $18d_p \times 18d_p \times 36d_p$, respectively. The slope of the linear portion of the discharge plot in Figure 2 gives the discharge rate. This figure shows that the discharge rate is almost independent of the domain size, provided it meets the minimum design constraint of $W > 2.5D$. This result is in good agreement with the findings of Brown and Richards,[28] who previously reported that the discharge rate remains constant as long as $W > 2.5D$.

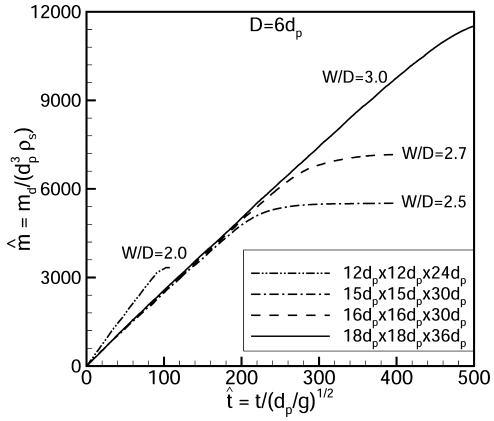

Figure 2. Effect of domain size on discharge rate from a flat-bottomed silo. Simulation parameters: $D = 6d_p$, $\mu_p = \mu_w = 0.1$, $e = 0.88$.

Parts a, b, and c of Figure 3 show contour plots of the magnitude of solid velocity [in $(d_p g)^{1/2}$ units] from the flat-bottomed silo at time $t = T_d/40$, $T_d/2$, and $3T_d/4$, respectively, where T_d is the discharge time scale (time required to completely discharge all the granular material from the silo). These figures show that the DEM simulations are able to capture the stagnant zones on the either side of the orifice, which has been previously observed experimentally by Nedderman et al.[21]

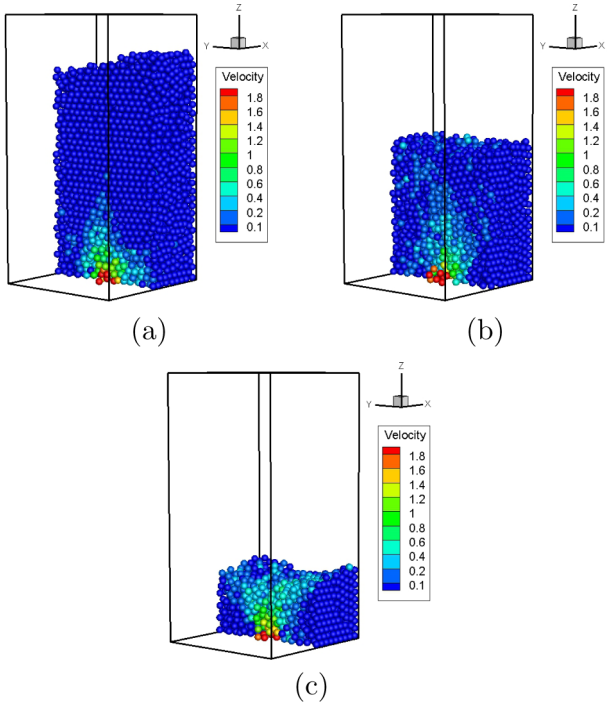

Figure 3. (a) Velocity contour [in $(d_p g)^{1/2}$ units] of particle discharge from silo at time $t = T_d/40$ (a), $T_d/2$ (b), and $3T_d/4$ (c).

dx.doi.org/10.1021/ie303598e | Ind. Eng. Chem. Res. 2013, 52, 13171−13182

2.2. Influence of Microscopic Parameters on Silo Discharge Rate. Both experimental[25] and DEM studies[5,7,8,26] have shown that friction can play an important role in determining granular rheology and, hence, could affect the discharge rate. However, the Beverloo correlation[18] [$\dot{m} = 0.58\rho_{bg}g^{0.5}(D - kd_p)^{2.5}$] has no dependence on friction (both interparticle and particle−wall). In order to quantify the influence of microscopic parameters (interparticle friction coefficient, particle−wall friction coefficient, and coefficient of restitution) on the discharge rate, we perform a series of 3D DEM simulations with different values of these parameters.

Figure 4 shows the time evolution of mass discharged (scaled with initial mass in the silo, m_0) for three different values of the interparticle friction coefficient: μ_p = 0.10, 0.25, and 0.50. The particle−wall friction coefficient is 0.10 in all the cases. This figure shows that as the coefficient of interparticle friction increases, the discharge rate decreases. The discharge rate decreases by about 30% when the interparticle friction coefficient increases from 0.1 to 0.5. These results indicate that the discharge rate depends on the interparticle friction coefficient, and its neglect in experimental correlations should be revisited. However, our DEM simulations reveal that the particle−wall friction coefficient has negligible influence on the discharge rate (results not shown here). Increasing the wall friction coefficient from 0.10 to 0.75 does not lead to any significant change in the silo discharge rate. This result can be attributed to the fact that, for a broad silo ($W/D \geq 2.5$), the wall friction coefficient does not affect the flow near the orifice outlet and, hence, has little effect on the discharge rate.

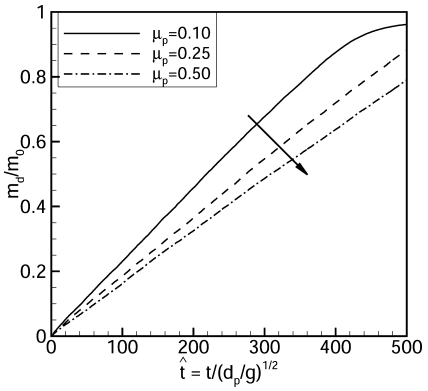

Figure 4. Amount of mass discharged (scaled with the initial mass in the silo, m_0) with time for three different values of interparticle friction coefficient. Simulation parameters: μ_w = 0.1, e = 0.88.

The coefficient of restitution is another parameter that has not been completely explored in experimental studies. In order to understand its influence on the discharge rate, we performed DEM simulations with different values of particle restitution coefficient ranging from 0.70 to 0.95. This range corresponds to the coefficient of restitution of particles generally used in solid processing industries. We find almost no change in the discharge rate when the particle restitution coefficient is increased from 0.70 to 0.95 (results not shown here). Using 2D simulations, Ristow[29] reported a change in the discharge rate of 1.2% when the coefficient of restitution increased from 0.5 to 0.9. This finding can be ascribed to the fact that silo flows are dense and are dominated by long-lasting, frictional, and multiparticle contacts. Hence, it is not surprising that the coefficient of restitution has a negligible influence on silo discharge dynamics.

2.3. Influence of System Parameters on Silo Discharge Rate. The Beverloo correlation of experimental data[18] shows that the discharge rate scales with the discharge outlet size to power 2.5 (see eq 27). This dependence of the discharge rate on the discharge outlet size is probed using 3D DEM simulations. In Figure 5a, the discharge rate is plotted with discharge outlet size ($\hat{D} = D/d_p$) for a simulation with an interparticle and particle−wall friction coefficient of 0.10. Figure 5a shows that the discharge rate is a function of outlet width raised to the power 2.4 for circular orifices, which matches extremely well with the Beverloo correlation, which predicts that the discharge rate scales with the outlet width raised to the power 2.5 for a 3D silo (see eq 27). Figure 5b shows the amount of mass discharged (scaled with the initial mass in the silo, m_0) with time for four different outlet sizes of $6d_p$, $7d_p$, $8d_p$, and $9d_p$. It is seen from Figure 5b that the discharge rate increases with an increase in the discharge outlet size, with an almost 4-fold increase as the discharge outlet size is increased from $6d_p$ to $9d_p$. Clearly, the discharge outlet size is one of the most important parameters influencing silo discharge.

2.4. Characterization of Different Regimes of Granular Rheology in Silo Discharge. As noted earlier, the rheology of granular flow depends on particle properties (friction

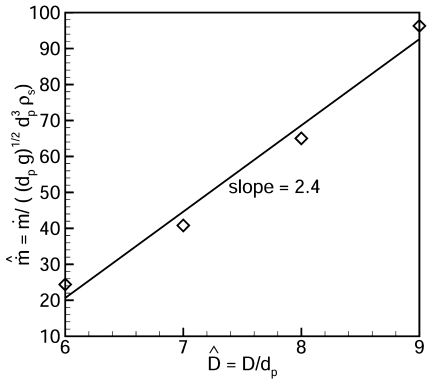

(a)

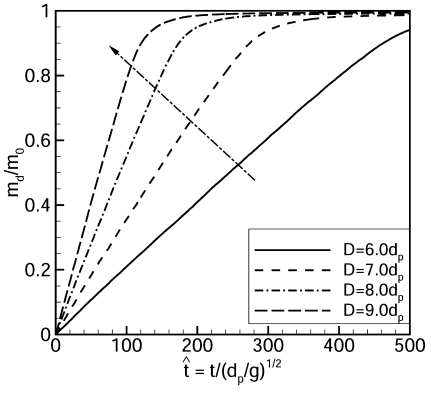

(b)

Figure 5. (a) Discharge rate with orifice outlet width. Simulation parameters: $\mu_p = \mu_w$ = 0.1, e = 0.88. (b) Amount of mass discharged (scaled with the initial mass in the silo, m_0) plotted with time for different widths of discharge outlets.

dx.doi.org/10.1021/ie303598e | Ind. Eng. Chem. Res. 2013, 52, 13171−13182

coefficient, coefficient of restitution) and macroscopic conditions of imposed shear rate and solid volume fraction. These different rheological behaviors are classified as different regimes of granular flow based on the scaling of shear stress with the strain rate.[5] In the inertial regime,[30] the stress scales as the square of the strain rate ($\sigma \propto \dot{\gamma}^2$), whereas in the quasi-static regime,[5] the stress remains independent of the strain rate [$\sigma \neq f(\dot{\gamma})$]. In between these two extremes there exists an intermediate regime where stress is related to the strain rate in the form of a power law ($\sigma \propto \dot{\gamma}^n$), where n takes values between 0 and 2 based on the interparticle friction coefficient and the shear rate.[4] In order to quantify the spatial extent of different regimes of granular rheology in this silo discharge problem, we first establish a regime map in the space of ν, μ_p, k^*; i.e., the parameter space defined by solid volume fraction ν, particle friction coefficient μ_p, and nondimensional shear rate $k^* = k_n/(\rho_s d_p{}^3 \dot{\gamma}^2)$. Different regimes of granular rheology (inertial, intermediate, and quasi-static) are identified on the basis of the scaling of shear stress with the strain rate using DEM data obtained from homogeneously sheared assemblies of granular particles (where the stress is independent of location), for a wide range of solid volume fractions, shear rates, and interparticle friction coefficients. Details about this comprehensive regime map can be found in previously published work.[26] These regimes have also been analyzed by other researchers.[7,8]

We now describe how the spatial extent of different granular rheology regimes is calculated from the DEM silo simulations. The interparticle friction coefficient μ_p is fixed in each DEM simulation, and we simulated $\mu_p = 0.5$ and $\mu_p = 0.25$ to represent a range of granular materials. In each DEM simulation, the solid volume fraction ν and nondimensional shear rate k^* vary spatially. The spatial map of granular rheology regimes is generated at the midplane of the silo, corresponding to $y = L/2$. The solid volume fraction and mean strain rate tensor

$$\dot{\gamma}_{ij} = \begin{bmatrix} \dot{\gamma}_{xx} & \dot{\gamma}_{xy} & \dot{\gamma}_{xz} \\ \dot{\gamma}_{yx} & \dot{\gamma}_{yy} & \dot{\gamma}_{yz} \\ \dot{\gamma}_{zx} & \dot{\gamma}_{zy} & \dot{\gamma}_{zz} \end{bmatrix}$$

are computed by averaging over cubical bins of side $2d_p$. The value of nondimensional shear rate k^* at the center of each bin is calculated using the second invariant of the mean strain rate tensor as

$$k^* = k_n/(\rho_s d_p{}^3 I_{2D}{}^2) \quad (1)$$

where

$$I_{2D} = \frac{1}{2}[[tr(\dot{\gamma})]^2 - tr(\dot{\gamma}^2)] \quad (2)$$

which is calculated from the components of the mean strain rate tensor as

$$I_{2D} = [(\dot{\gamma}_{xx}\dot{\gamma}_{yy} + \dot{\gamma}_{yy}\dot{\gamma}_{zz} + \dot{\gamma}_{xx}\dot{\gamma}_{zz}) - (\dot{\gamma}_{xy}\dot{\gamma}_{yx} + \dot{\gamma}_{xz}\dot{\gamma}_{zx} + \dot{\gamma}_{yz}\dot{\gamma}_{zy})] \quad (3)$$

Using the values of ν, μ_p, and k^* at each bin center, we assign that location a value corresponding to its regime: 2 for inertial, 1 for intermediate, and 0 for quasi-static according to the regime map established by Vidyapati and Subramaniam.[26] Parts a and b of Figure 6 show the spatial extent of different regimes

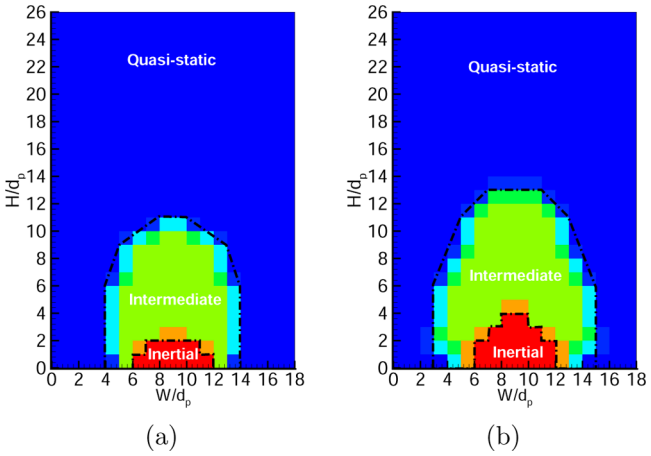

Figure 6. Characterization of spatial extent of different regimes of granular rheology in a flat-bottomed silo based on local solid volume fraction, mean strain rate, and particle friction coefficient. Blue represents the quasi-static regime and red represents the inertial (rapid flow) regime, whereas other colors indicate the spatial extent of the intermediate regime. (a) Simulation parameters: $D = 6d_p$, $\mu_p = 0.5$, $e = 0.91$. (b) Simulation parameters: $D = 6d_p$, $\mu_p = 0.25$, $e = 0.91$.

in a flat-bottomed silo obtained using this method for interparticle friction coefficient values of 0.50 and 0.25, respectively. In Figure 6a,b, red represents the inertial regime (which is found to exist near the discharge orifice), blue indicates the quasi-static regime (which exists near walls and regions far away from the discharge outlet), and the presence of any other color corresponds to the intermediate regime.

From this study, it is evident that all three regimes of granular rheology (inertial, intermediate, and quasi-static) coexist for this silo discharge problem. It is also interesting to note that the intermediate regime spans a considerable spatial region in the silo. Comparing parts b ($\mu_p = 0.25$) and a ($\mu_p = 0.5$) of Figure 6 reveals that the spatial extent of the intermediate regime expands as the interparticle friction coefficient decreases from 0.50 to 0.25. The interparticle friction coefficient for most granular materials (such as glass beads) used in the solid processing industries varies between 0.15 and 0.50, and hence, expansion of the intermediate regime has implications for granular flow in practical devices. This result also indicates that it is critical to understand the rheological behavior of the intermediate regime, which still poses significant challenges for constitutive models.[26] Most of the frequently used constitutive models do not perform satisfactorily in this regime.

3. CONTINUUM SIMULATIONS

A continuum description of granular flow is useful for simulating problems at a larger industrial scale, but they require accurate constitutive models. To perform a quantitative assessment of different constitutive models, we compare the discharge rates, solid velocities, and solid stresses obtained from DEM and continuum simulation of a 3D silo.

3.1. Setup for Continuum Simulations. Simulations of particle discharge from a 3D flat-bottomed silo are performed using the averaged two-fluid (TF) continuum formulation in the MFIX computer code.[19] MFIX is an Eulerian−Eulerian computational fluid dynamics (CFD) model in which gas and granular solids are modeled as continua. However, since the current study focuses only on dense granular flows, the effect of

dx.doi.org/10.1021/ie303598e | Ind. Eng. Chem. Res. 2013, 52, 13171−13182

interstitial fluid can be neglected (provided the particle diameters are relatively large, e.g., Geldart type B particles). Therefore, no effect of fluid is introduced in the MFIX model equations. The "dry" granular kinetic theory model used in the MFIX code[19] is essentially the same as that derived by Lun et al.[9] Conservation of mass for constant solid density results in

$$\rho_s\left[\frac{\partial \nu}{\partial t} + \nabla\cdot(\nu \mathbf{v}_s)\right] = 0 \tag{4}$$

where ρ_s is the solid density, ν is the solid volume fraction, and $\mathbf{v}_s$ is the average solid-phase velocity. Conservation of linear momentum is given by

$$\rho_s\left[\frac{\partial \nu \mathbf{v}_s}{\partial t} + \nabla\cdot(\nu \mathbf{v}_s\mathbf{v}_s)\right] = \nabla\cdot(\boldsymbol{\tau}_k + \boldsymbol{\tau}_f) + \nu\rho_s\mathbf{g} \tag{5}$$

where $\boldsymbol{\tau}_k$ and $\boldsymbol{\tau}_f$ are the kinetic and frictional part of the stress tensor, respectively. The translational granular energy conservation equation is given by

$$\frac{3}{2}\rho_s\left[\frac{\partial \nu\Theta_s}{\partial t} + \nabla\cdot(\nu\Theta_s\mathbf{v}_s)\right] = -\nabla\cdot\mathbf{q} + \boldsymbol{\tau}_k\colon\nabla\mathbf{v}_s - \rho_s J_s \tag{6}$$

where Θ_s is the granular temperature, $\mathbf{q}$ is the flux of granular energy, and J_s is the granular energy dissipation due to inelastic collisions. Solids kinetic−collisional and frictional stress terms are given by

$$\boldsymbol{\tau}_k = [-P_s + \eta\mu_b\nabla\cdot\mathbf{v}_s]\mathbf{I} + 2\mu_s\mathbf{S}_S \tag{7}$$

$$\boldsymbol{\tau}_f = -P_f\mathbf{I} + 2\mu_f\mathbf{S}_S \tag{8}$$

and

$$\mathbf{S}_S = \frac{1}{2}[\nabla\mathbf{v}_s + (\nabla\mathbf{v}_s)^T] - \frac{1}{3}\nabla\cdot\mathbf{v}_s\mathbf{I} \tag{9}$$

where P_s is the solid pressure, η is a constant depending on the particle restitution coefficient,[20] μ_b is the bulk viscosity of the solid phase, $\mathbf{I}$ is the identity tensor, μ_s is the granular viscosity, and $\mathbf{S}_S$ is the strain rate tensor as given in eq 9. The closures for different terms arising from the kinetic theory are taken from Lun et al.,[9] while three different constitutive models for the frictional stress are used.

The problem studied is a 3D flat-bottomed silo with domain size 18 × 18 × 36 particle diameters in x, y, and z directions, respectively, with an open top and an orifice centered at the bottom. The only difference between the continuum and DEM simulations is that the continuum simulations have a square-shaped outlet, whereas the DEM simulations have a circular outlet. However, the effective diameter (hydraulic diameter) of the square discharge outlet is the same as the diameter of the circular outlet, which is $6d_p$. A $5d_p$ high region below the silo is included in the domain so that a boundary condition is not required right at the exit of the bin. A grid resolution of d_p, d_p, and $2d_p$ is used in the x, y, and z directions, respectively. According to Srivastava and Sundaresan,[20] such a fine mesh is required to effectively resolve variations in the velocities and solid volume fractions near the orifice region. The initial solid volume fraction in the bin is set to 0.60, whereas the initial granular temperature is taken to be nonzero everywhere ($0.01d_pg$ units). Table 1 lists the values of the simulation parameters used for the flat-bottomed silo simulations.

The boundary condition for momentum and pseudo-thermal energy (PTE) of the particulate phase at the walls of the silo are taken from Johnson and Jackson.[31] This boundary condition can be written as

$$\mathbf{n}\cdot(\boldsymbol{\tau}_k + \boldsymbol{\tau}_f)\cdot\frac{\mathbf{v}_{sl}}{|\mathbf{v}_{sl}|} + (\mathbf{n}\cdot\boldsymbol{\tau}_f\cdot\mathbf{n})\tan\delta + \frac{\pi\sqrt{3}}{6\nu^{max}}\phi'\rho_s\nu g_0\Theta_s^{1/2}\mathbf{v}_{sl} = 0 \tag{10}$$

$$\mathbf{n}\cdot\mathbf{q} = \frac{\pi\sqrt{3}}{6\nu^{max}}\phi'\rho_s\nu g_0\Theta_s^{1/2}|\mathbf{v}_{sl}|^2 - \frac{\pi\sqrt{3}}{4\nu^{max}}(1 - e_w^{\,2})\rho_s\nu g_0\Theta_s^{3/2} \tag{11}$$

where $\mathbf{n}$ is the unit normal from the boundary into the particle assembly, $\boldsymbol{\tau}_k$ and $\boldsymbol{\tau}_f$ are the kinetic and frictional stress tensors, respectively, ν^{max} is the maximum solid volume fraction, Θ_s is the granular temperature, $\mathbf{q}$ is the flux of granular energy, δ is the angle of wall friction for the material, ϕ' is the specularity coefficient, ρ_s is the solid density, ν is the solid volume fraction, e_w is the coefficient of restitution at the wall, and $\mathbf{v}_{sl} = \mathbf{v} - \mathbf{v}_{wall}$ is the slip velocity of the particle assembly at the wall. For all other dependent variables, the usual continuation condition (i.e., zero gradient in the direction normal to the boundary) is applied. The silo is initialized with particles at rest, corresponding to an initial void fraction of 0.40.

Table 1. Values of Model Parameters Used in the Continuum Simulations

parameter	values
solid density, ρ_s	2.9 g/cm^3
particle diameter, d_p	1 mm
angle of internal friction, ϕ	26.56
angle of wall friction, δ	12.3
specularity coefficient, ϕ'	0.25
interparticle coefficient of restitution, e	0.91
coefficient of restitution at wall, e_w	0.91
maximum solid packing, ν^{max}	0.65

3.2. Description of Constitutive Models. Three different constitutive models (Schaeffer,[12] S&S,[20] and CSS[7]) for the frictional stress are used to simulate silo discharge in this work. The continuum simulation results corresponding to the Schaeffer and S&S models in section 3.3 refer to an implementation where the total granular stress is decomposed into a kinetic part, τ_k (obtained from the kinetic theory of granular flow[9]) and a frictional part τ_f due to enduring contacts obtained from the Schaeffer or S&S models, as implied by eq 5. A brief description of these models is presented below.

3.2.1. Schaeffer Model.[12] This model has been traditionally used in the MFIX code.[19] It is used when the critical state is reached, where the solid volume fraction exceeds the maximum packing limit. In the Schaeffer model,[12] I_{2D} represents the second invariant of the deviator of the strain rate tensor, which is related to the norm of the square of the strain rate tensor by $I_{2D}^{1/2} = (\mathbf{S}_s\colon\mathbf{S}_s)^{1/2}/2$. The model for the frictional stresses is given by the following equations:[17]

$$P_f = P_c = \begin{cases} 10^{25}(\nu - \nu^{max})^{10} & \text{if } \nu > \nu^{max} \\ 0 & \text{if } \nu \le \nu^{max} \end{cases} \tag{12}$$

$$\mu_f = \begin{cases} \dfrac{P_c}{2\sqrt{I_{2D}}}\sin(\phi) & \text{if } \nu > \nu^{max} \\ 0 & \text{if } \nu \le \nu^{max} \end{cases} \tag{13}$$

dx.doi.org/10.1021/ie303598e | Ind. Eng. Chem. Res. 2013, 52, 13171−13182

where P_c is the critical state pressure, $\mathbf{S}_S$ is the strain rate tensor, and ν and ν^{max} are the solid volume fraction and its value at the maximum packing limit, respectively.

3.2.2. S&S Model.[20] This frictional model is proposed by Srivastava and Sundaresan,[20] who gave expressions for the frictional stresses in a compressible granular assembly. This model is a modification of Savage's model[32] that accounts for strain rate fluctuations even in the dense regime of granular flow. The frictional stresses start influencing the granular flow at a minimum solid volume fraction (ν^{min}), which is below the maximum packing (ν^{max}), as proposed by Johnson and Jackson.[31] In this study, the critical state theory applies only when the granular assembly is incompressible (i.e., above maximum packing). The critical state pressure in the S&S model[20] is specified by the following equation:

$$P_c = \begin{cases} 10^{25}(\nu - \nu^{max})^{10} & \text{if } \nu > \nu^{max} \\ Fr\dfrac{(\nu - \nu^{min})^r}{(\nu^{max} - \nu)^s} & \text{if } \nu^{max} \geq \nu > \nu^{min} \\ 0 & \text{if } \nu \leq \nu^{min} \end{cases} \tag{14}$$

where $Fr = 0.5$ dyn/cm^2. Typical values for the model constants r and s are chosen to be $r = 2$ and $s = 5$ in this model.[20] The frictional pressure is related to the critical state pressure as follows:

$$\frac{P_f}{P_c} = \left(1 - \frac{\nabla\cdot\mathbf{v}_s}{n\sqrt{2}\,\sin(\phi)\sqrt{\mathbf{S}_S:\mathbf{S}_S + \Theta_s/{d_p}^2}}\right)^{n-1} \tag{15}$$

$$\mu_f = \frac{\sin(\phi)}{\sqrt{2}}\frac{P_f}{\sqrt{\mathbf{S}_S:\mathbf{S}_S + \Theta_s/{d_p}^2}}\left(n - (n-1)\left(\frac{P_f}{P_c}\right)^{1/(n-1)}\right) \tag{16}$$

The coefficient n has different values depending on whether the granular assembly is experiencing a dilation or compaction:

$$n = \begin{cases} \dfrac{\sqrt{3}}{2}\sin(\phi) & \text{if } \nabla\cdot\mathbf{v}_s \geq 0 \\ 1.03 & \text{if } \nabla\cdot\mathbf{v}_s < 0 \end{cases} \tag{17}$$

In eq 17, the coefficient n determines the shape of the yield surface.

3.2.3. CSS (Chialvo–Sun–Sundaresan) Model.[7] The general form of this recently developed CSS bridging model can be written as[7]

$$p = \begin{cases} p_{QS} + p_{Int} & \text{for } \nu \geq \nu_c \\ ({p_{Inert}}^{-1} + {p_{Int}}^{-1})^{-1} & \text{for } \nu < \nu_c \end{cases} \tag{18}$$

$$\tau = \begin{cases} \tau_{QS} + \tau_{Int} & \text{for } \nu \geq \nu_c \\ ({\tau_{Inert}}^{-1} + {\tau_{Int}}^{-1})^{-1} & \text{for } \nu < \nu_c \end{cases} \tag{19}$$

In eqs 18 and 19, the subscripts QS, Int, and Inert correspond to the quasi-static, intermediate, and the inertial regime, respectively. Here ν and ν_c are the solid volume fraction and critical solid volume fraction, respectively. In eqs 18 and 19, the individual regime contributions are defined as

$$p_{QS} = \alpha_{QS}|\nu - \nu_c| \tag{20}$$

$$p_{Int} = \alpha_{Int}\hat{\dot{\gamma}}^{2/3} \tag{21}$$

$$p_{Inert} = \frac{\alpha_{Inert}\hat{\dot{\gamma}}^2}{|\nu - \nu_c|^2} \tag{22}$$

$$\tau_{QS} = \beta_{QS}|\nu - \nu_c| \tag{23}$$

$$\tau_{Int} = \beta_{Int}\hat{\dot{\gamma}}^{5/7} \tag{24}$$

$$\tau_{Inert} = \frac{\beta_{Inert}\hat{\dot{\gamma}}^2}{|\nu - \nu_c|^{9/5}} \tag{25}$$

where $\hat{\dot{\gamma}}$ is defined as follows:

$$\hat{\dot{\gamma}} = \frac{\dot{\gamma}d_p}{\sqrt{k_n/(\rho_s d_p)}} = \sqrt{\frac{1}{k^*}} \tag{26}$$

In eq 26, $k^* = k_n/(\rho_s {d_p}^3\dot{\gamma}^2)$ is the nondimensional shear rate, $\dot{\gamma}$ is the applied shear rate, k_n is the normal spring constant, d_p is the particle diameter, and ρ_s is the solid particle density. The model constants α_{QS}, β_{QS}, α_{Int}, β_{Int}, α_{Inert}, and β_{Inert} are specified in Table 2 on the basis of the work of Chialvo et al.[7]

Table 2. CSS Model Constants Corresponding to Different Regimes of Granular Flow

model constant	value
α_{QS}	$0.676(k_n/d_p)$
β_{QS}	$0.260(k_n/d_p)$
α_{Int}	$0.15k_n(\rho_s/k_n)^{1/3}$
β_{Int}	$0.0854(k_n/d_p)(\rho_s {d_p}^3/k_n)^{5/14}$
α_{Inert}	$0.0185({d_p}^2\rho_s)$
β_{Inert}	$0.0217({d_p}^2\rho_s)$

3.3. Quantitative Comparison between DEM and Continuum Simulations of Silo Discharge. The discharge rate is one of the most important quantities measured in silos. Figure 7a shows the temporal variation of the discharge rate for a 3D flat-bottomed silo. This result shows that at early time there is a rapid increase in the discharge rate, which is then followed by a plateau region, where the discharge rate does not vary appreciably with time. Figure 7a also shows that the steady discharge obtained from the Schaeffer model is 7.75 g/s, whereas the steady discharge obtained from the S&S model is 9.62 g/s. This difference in the prediction of discharge rate is attributed to the fact that, in the S&S model, the frictional stress starts influencing the granular flow at a value of solid volume fraction (ν^{min} in the description of S&S model) that is lower than the Schaeffer model, where frictional effects only start at maximum packing.[17] However, the CSS model[7] predicts a discharge rate of 6.67 g/s. We also compute the discharge rate from DEM simulation and the Beverloo correlation and compare these with the discharge rate obtained from different constitutive models. These calculations are done for particles with a density of 2.9 g/cm^3 and 1 mm diameter. For these particle properties, DEM predicts a steady discharge rate of 4.94 g/s (shown with dash–dot–dot line in Figure 7a). The Beverloo correlation (eq 27)

dx.doi.org/10.1021/ie303598e | Ind. Eng. Chem. Res. 2013, 52, 13171–13182

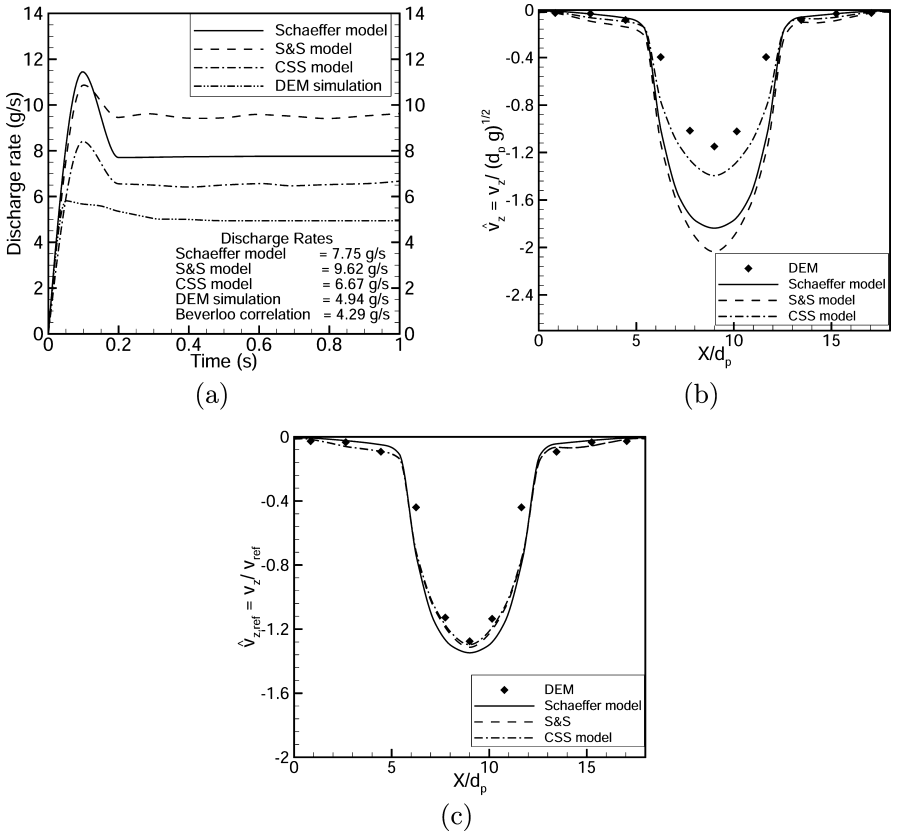

Figure 7. (a) Temporal variation of the discharge rate using three different constitutive models and DEM simulations for a 3D flat-bottomed silo. (b) Profile of vertical component of solid velocity near the orifice during steady discharge, and (c) same as in part b but normalized by the reference velocity $v_{ref} = \dot{m}/(\rho_b A)$ based on the discharge rate corresponding to each model. Simulation parameters: $D = 6d_p$, $\mu_p = 0.5$, $e = 0.91$.

$$\dot{m} = 0.58\rho_b g^{0.5}(D - kd_p)^{2.5} \tag{27}$$

predicts a discharge rate of 4.29 g/s. In eq 27, $\dot{m}$ is the discharge rate, $\rho_b = \rho_s\nu$ is the initial solid bulk density, g is the acceleration due to gravity, D is the outlet discharge size, k is the Beverloo constant, and d_p is the particle diameter. From this result it is evident that the two frequently used constitutive models (Schaeffer and S&S) significantly overpredict the discharge rate compared to the discharge rate obtained from the Beverloo correlation[18] and DEM data. The CSS model does somewhat better by predicting the discharge rate within 35% of DEM data. However, there is good agreement between the discharge rate predicted using DEM simulations and the Beverloo correlation of experimental data.

The discharge rate is closely related to the discharge velocity of solids near the orifice, and these are compared in Figure 7b. The vertical component of solid velocity is extracted during steady discharge at a location $2d_p$ above the bottom orifice. As shown in Figure 7b, the velocity of solid particles is highest at the center of the orifice for all the constitutive models and DEM simulations. Near the walls the particles flow down with very low velocity, as seen in Figure 7b. As expected, the discharge velocity predicted by the S&S model is higher than the discharge velocity computed using the Schaeffer and CSS models, thus leading to the higher discharge rate prediction by the S&S model, as shown in Figure 7a. The discharge velocity predicted by the DEM simulation is lowest, which also verifies the lower discharge rate predicted by the DEM simulation. Figure 7c shows the vertical component of solid velocity normalized by the reference velocity $[v_{ref} = \dot{m}/(\rho_b A)]$ based on the discharge rate corresponding to each model. This figure shows that the models predict a similar shape of the velocity profile, but there are quantitative differences in the discharge rate prediction, as shown in Figure 7a.

In order to understand this discrepancy in the discharge rate prediction, the error incurred in the solid stress prediction is quantified by comparing the predicted granular stress (using the three different constitutive models) with that of DEM data. We extract stresses from the constitutive models and DEM simulations in each cell and quantify the error using the vector norm of the relative error in each cell:

$$\hat{\varepsilon} = \frac{\left\|(\sigma_{ij})_{model} - (\sigma_{ij})_{DEM}\right\|_2}{\left\|(\sigma_{ij})_{DEM}\right\|_2} \tag{28}$$

In the DEM, these stresses are extracted in a slice of thickness $2d_p$ in the y direction, which is located at the center of the silo. A uniform grid with spacing $2d_p \times 2d_p$ is used in the x (along the width of the silo) and z (along the height of the silo) directions to perform this error analysis. Parts a, b, and c in Figure 8 are the contour plots of error ($\hat{\varepsilon}$) in solid stress prediction using Schaeffer, S&S, and CSS models, respectively. This figure shows that the maximum error incurred in solid stress prediction (when compared with the stresses computed from DEM simulations) is around 42% and 56% for the Schaeffer and S&S model, respectively. However, the CSS model[7] is able to predict solid stresses within 26% of the DEM data. The better performance of the CSS model is ascribed to the fact that this model provides a blending function for

dx.doi.org/10.1021/ie303598e | Ind. Eng. Chem. Res. 2013, 52, 13171−13182

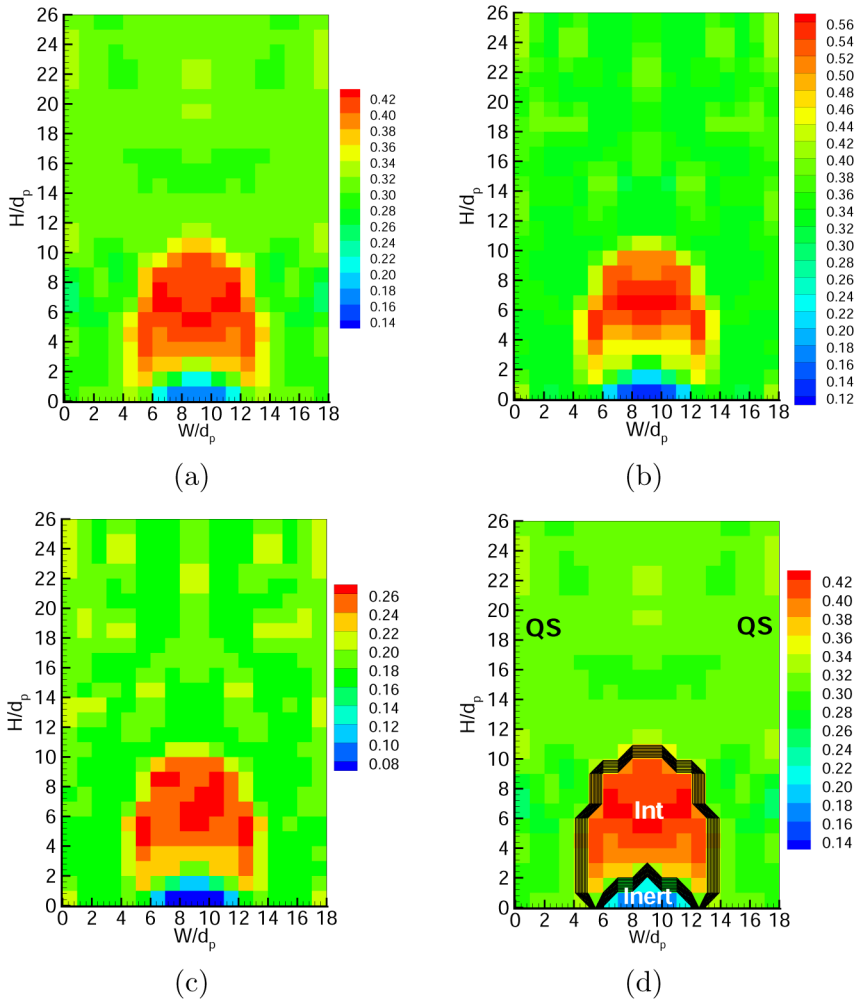

Figure 8. Error in solid stress prediction (error quantified using vector norm of relative error, see eq 28): (a) for the Schaeffer model, (b) for the S&S model, (c) for the CSS model, and (d) for the Schaeffer model superimposed with the spatial extent of different regimes (QS, quasi-static; Int, intermediate; Inert, inertial) of granular rheology. Simulation parameters: $D = 6d_p$, $\mu_p = 0.5$, $e = 0.91$.

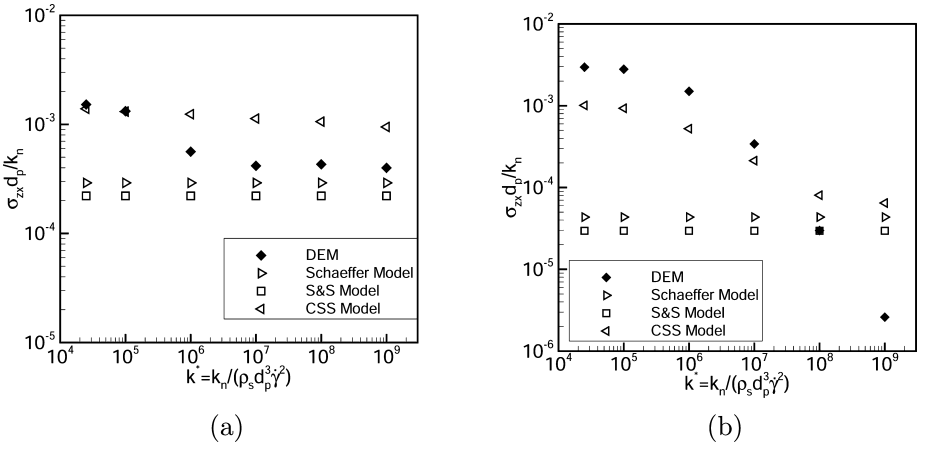

Figure 9. Performance of different continuum models in a simple homogeneous shear flow. (a) Simulation parameter: $\nu = 0.62$, $\mu_p = 0.1$, and $e = 0.7$. (b) Simulation parameter: $\nu = 0.58$, $\mu_p = 1.0$, and $e = 0.7$.

patching each regime's asymptotic form in order to predict the stresses in different regimes of granular rheology.

It is also interesting to note that the S&S model predicts the lowest stresses (both shear as well as normal stresses). The reason for this lower stress prediction by the S&S model is attributed to fact that the S&S model allows for the dilation effect at solid volume fractions below the critical packing value. In the S&S model the frictional pressure is modified for the dilation effect, as opposed to directly using its value at the critical state (which assumes the granular assembly deforms without any volume change) as done by Schaeffer. In the Schaeffer model, high values of frictional viscosity are expected

dx.doi.org/10.1021/ie303598e | Ind. Eng. Chem. Res. 2013, 52, 13171−13182

due to the high critical pressure computed using eq 12. The S&S model predicts a frictional pressure (P_f) that is always lower than the critical pressure (P_c) if the assembly is dilating ($\nabla\cdot\mathbf{v}_s > 0$ in eq 15). Therefore, the stresses computed in the S&S model are lower than that of the Schaeffer and CSS models. Figure 8d shows the error in solid stress prediction (for the Schaeffer model) superimposed on the spatial extent of different regimes of granular rheology for an interparticle friction coefficient of 0.5. In Figure 8d QS, Int, and Inert correspond to the quasi-static, intermediate, and the inertial regimes of granular rheology, respectively. This figure shows that the maximum error incurred in the solid stress prediction corresponds almost exactly to the spatial region where the intermediate regime is present. Therefore, it can be concluded that this intermediate regime poses a significant challenge for the constitutive models. Note that in the intermediate regime, the scaling of stress with strain rate is $\sigma \propto \dot{\gamma}^n$ $(0 < n < 2)$, where n is itself a function of particle (such as interparticle friction coefficient, coefficient of inelasticity) and flow (such as the shear rate) properties.

To further investigate the performance of these three constitutive models in the intermediate regime of granular rheology, where the error in solid stress prediction is found to be highest, we compare their shear stress predictions with DEM data for homogeneously sheared granular flow. These homogeneous shear simulations are performed with periodic boundary conditions in all directions (x, y, and z) and uniform shear is generated in the domain using the "SLLOD" algorithm.[33] The SLLOD algorithm[33] is used in conjunction with the Lees−Edwards boundary condition[34] to generate simple shear flows.

Parts a and b of Figure 9 show the comparison of the shear stress predicted using these three constitutive models with DEM data for a solid volume fraction of 0.62 and 0.58 with an interparticle friction coefficient of 0.1 and 1.0, respectively (it is established by Vidyapati and Subramaniam[26] that this combination of solid volume fraction and particle friction coefficient can exhibit intermediate regime flow behavior over a range of shear rates). These values also correspond to the range of solid volume fraction values (0.57−0.62) that was extracted from the continuum simulations in the spatial region corresponding to the intermediate regime. Both parts of Figure 9 show that the shear stress predicted using the Schaeffer[12] and the S&S[20] models are almost independent of the applied shear rate in the intermediate regime. The CSS model[7] shows a dependence on shear rate, but it does not accurately capture the DEM data for all values of the shear rate tested in the intermediate regime. This result reveals that the constitutive models used in the continuum description of granular flows in this work are not able to quantitatively predict the DEM data for rheological behavior of stress with the strain rate in the intermediate regime, although the CSS model is best able to capture the qualitative trends.

4. CONCLUSIONS

Discharge dynamics of granular particles from a 3D flat-bottomed silo is studied using both discrete (DEM) and continuum simulations. DEM results for discharge rate in a flat-bottomed silo are shown to behave robustly with variation of parameters such as interparticle friction coefficient and discharge outlet size. However, it is found that the wall friction coefficient and particle coefficient of restitution have no influence on the discharge rate. The spatial extent of different regimes of granular rheology in the silo discharge problem is quantified using a regime map established from DEM simulation data of homogeneously sheared granular flow.[26] The results of this study reveal that all three regimes of granular rheology (inertial, intermediate, and quasi-static) coexist in this silo discharge problem. It is also found that the spatial extent of the intermediate regime that occupies a significant portion of the solid flow directly above the orifice expands as the interparticle friction coefficient decreases.

Quantitative comparison of DEM and different constitutive models in the continuum simulations reveals that two frequently used constitutive models (Schaeffer[12] and S&S[20]) significantly overpredict the discharge rate from the silo. However, the CSS model[7] does somewhat better by predicting a discharge rate within 35% of the DEM data. Nevertheless, the DEM prediction of discharge rate is in very good agreement with the discharge rate computed using the Beverloo correlation[18] of experimental data. The error in the solid stress (with respect to DEM data) incurred by the constitutive models shows a maximum of 42%, 56%, and 26% for the Schaeffer, S&S, and CSS models, respectively. It is also found that the spatial region with the maximum error (for all the constitutive models used in this study) in the solid stress prediction almost exactly overlaps the region corresponding to the intermediate regime of granular rheology. The results of this study reconfirm that DEM can be used as a tool to isolate and identify one of the possible causes for poor prediction of the discharge rate in silos, namely, the large spatial extent of the intermediate regime and its complex rheological behavior, which current constitutive models have difficulty in capturing.

APPENDIX: CONTACT MODEL DESCRIPTION

For two contacting particle $\{i,j\}$, with radii $\{a_i,a_j\}$ at positions $\{\mathbf{r}_i,\mathbf{r}_j\}$, with velocities $\{\mathbf{v}_i,\mathbf{v}_j\}$, and angular velocities $\{\boldsymbol{\omega}_i, \boldsymbol{\omega}_j\}$, the normal compression (δ_{ij}), relative normal velocity ($\mathbf{v}_{n_{ij}}$), and relative tangential velocity ($\mathbf{v}_{t_{ij}}$) are[3]

$$\delta_{ij} = d_p - r_{ij} \tag{A.1}$$

$$\mathbf{v}_{n_{ij}} = (\mathbf{v}_{ij}\cdot\mathbf{n}_{ij})\mathbf{n}_{ij} \tag{A.2}$$

$$\mathbf{v}_{t_{ij}} = \mathbf{v}_{ij} - \mathbf{v}_{n_{ij}} - (a_i\boldsymbol{\omega}_i + a_j\boldsymbol{\omega}_j) \times \mathbf{n}_{ij} \tag{A.3}$$

where $d = a_i + a_j$, $\mathbf{r}_{ij} = \mathbf{r}_i - \mathbf{r}_j$, $\mathbf{n}_{ij} = \mathbf{r}_{ij}/r_{ij}$, with $r_{ij} = |\mathbf{r}_{ij}|$ and $\mathbf{v}_{ij} = \mathbf{v}_i - \mathbf{v}_j$.

Note that there is no sum over repeated indices. The rate of change of the elastic tangential displacement ($\mathbf{u}_{t_{ij}}$), set to zero at the initiation of contact, is

$$\frac{d\mathbf{u}_{t_{ij}}}{dt} = \mathbf{v}_{t_{ij}} - \frac{(\mathbf{u}_{t_{ij}}\cdot\mathbf{v}_{ij})\mathbf{r}_{ij}}{r_{ij}^2} \tag{A.4}$$

The last term in eq A.4 arises from the rigid body rotation around the contact point and ensures that $\boldsymbol{u}_{tij}$ always lies in the local tangent plane of contact. Normal and tangential forces acting on particle i are

$$\mathbf{F}_{n_{ij}} = f(\delta_{ij}/d_p)(k_n\delta_{ij}\mathbf{n}_{ij} - \gamma_n m_{eff}\mathbf{v}_{n_{ij}}) \tag{A.5}$$

$$\mathbf{F}_{t_{ij}} = f(\delta_{ij}/d_p)(-k_t\mathbf{u}_{t_{ij}} - \gamma_t m_{eff}\mathbf{v}_{t_{ij}}) \tag{A.6}$$

where $k_{n,t}$ and $\gamma_{n,t}$ are the spring stiffness and viscoelastic constants, respectively, and $m_{eff} = m_i m_j/(m_i + m_j)$ is the reduced

mass of spheres with masses m_i and m_j. In this work, all particles have the same mass, m_p. The corresponding contact force on particle j is simply given by Newton's third law, i.e., $\mathbf{F}_{ji} = -\mathbf{F}_{ij}$. The function $f(\delta_{ij}/d_p) = 1$ is for the linear spring−dashpot model, and $f(\delta_{ij}/d_p) = (\delta_{ij}/d_p)^{1/2}$ is for Hertzian contacts with viscoelastic damping between spheres. Static friction is implemented by keeping track of the elastic shear displacement throughout the lifetime of a contact. The static yield criterion, characterized by a local particle friction coefficient μ, is modeled by truncating the magnitude of $\mathbf{u}_{t_{ij}}$ as necessary to satisfy $|\mathbf{F}_{t_{ij}}| < |\mu\mathbf{F}_{n_{ij}}|$. Thus, the contact surfaces are treated as "sticking" when $|\mathbf{F}_{t_{ij}}| < |\mu\mathbf{F}_{n_{ij}}|$ and as "slipping" when the yield criterion is satisfied.

The amount of energy lost in collisions is characterized by the value of the coefficient of restitution, which is defined as the negative ratio of the particle normal velocity after collision to the velocity before collision. For the linear spring−dashpot model, the coefficient of normal restitution and contact time can be analytically obtained

$$e_n = e^{-\gamma_n t_c/2} \tag{A.7}$$

where the contact time (t_c) is given by

$$t_c = \pi(k_n/m_{eff} - \gamma_n^2/4)^{-1/2} \tag{A.8}$$

The value of the spring constant should be large enough to avoid particle interpenetration yet not so large as to require an unreasonably small simulation time step dt, since an accurate simulation typically requires $dt \sim t_c/50$.[5] After the contact force is calculated, the equations of motion, which are ordinary differential equations, can be numerically integrated to get the particle trajectories.

The total granular stress corresponding to the DEM contact force model is composed of contact (virial) and streaming (dynamic) contributions that can be computed from particle properties in a domain of volume V as

$$\boldsymbol{\sigma} = \boldsymbol{\sigma}^{\text{contact}} + \boldsymbol{\sigma}^{\text{streaming}} = \frac{1}{V}\sum_{i}^{N}\left[\sum_{j,j\neq i}\frac{1}{2}\mathbf{r}^{(i)(j)} \otimes \mathbf{f}^{(i)(j)} + (m_p\mathbf{v}'^{(i)} \otimes \mathbf{v}'^{(i)} + I\boldsymbol{\omega}'^{(i)} \otimes \boldsymbol{\omega}'^{(i)})\right] \tag{A.9}$$

where $\mathbf{r}^{(i)(j)}$ is the vector pointing from the center of particle j to the center of particle i, $\mathbf{f}^{(i)(j)}$ is the contact force acting on particle i by particle j, m_p is the mass of a particle, $I = m_p d_p^2/4$ is the moment of inertia of a spherical particle about its center, $\mathbf{v}'$ is the fluctuating velocity, $\boldsymbol{\omega}'$ is the fluctuation in particle rotational velocity, and $\otimes$ denotes a dyadic product. The stress obtained from DEM simulations in this paper neglects the final term associated with the rotational momentum transfer, and only the virial and translational terms are included. However, sample calculations of stress including the rotational momentum transfer term indicate that the difference in total stress is less than 1% for solid volume fraction values greater than 0.53. Therefore, its neglect does not significantly change the results or conclusions of this paper.

AUTHOR INFORMATION

Corresponding Author

*E-mail: shankar@iastate.edu.

Present Address

[†]Corporate Engineering Technology Laboratory, The Procter & Gamble Co., 8256 Union Centre Blvd, West Chester, OH 45069.

Notes

The authors declare no competing financial interest.

ACKNOWLEDGMENTS

The authors wish to acknowledge the financial support from U.S. Department of Energy National Energy Technology Laboratory (grant DE-FG26-07NT43070), administered under Advanced Coal Research at U.S. colleges and universities. The authors also acknowledge graduate student Ravi Kolakaluri for his help with some of the figures.

NOMENCLATURE

$\dot{m}$ discharge rate
D size of discharge outlet
d_p particle diameter
e particle restitution coefficient
e_w coefficient of restitution at wall
H fill height at silo centerline
J_s granular energy dissipation due to inelastic collision
k Beverloo constant
k^* nondimensional shear rate
k_n particle normal stiffness coefficient
m_0 initial mass in silo
m_d amount of mass discharged from silo
m_p particle mass
n coefficient in the frictional model
P_c critical state pressure
P_f frictional pressure
P_s solid pressure
t_c binary collision time
T_d discharge time scale
W silo width
$\mathbf{g}$ acceleration due to gravity
$\mathbf{I}$ identity tensor
$\mathbf{q}$ flux of granular energy
$\mathbf{v}_s$ solid velocity
Δt time step for DEM simulations

Greek symbols

δ angle of wall friction
$\dot{\gamma}$ shear rate
η constant depending on particle restitution coefficient
μ_b bulk viscosity of solid phase
μ_f frictional viscosity
μ_g gas viscosity
μ_p particle friction coefficient
μ_s granular viscosity
μ_w wall friction coefficient
ν solid volume fraction
ν^{max} maximum solid packing
ϕ angle of internal friction
ϕ' specularity coefficient
ρ_b bulk density of solid
ρ_g gas density
ρ_s particle density
σ granular stress

Θ_s granular temperature
τ_f frictional part of stress tensor
τ_k kinetic part of stress tensor
ν^{min} minimum frictional solid volume fraction

REFERENCES

(1) Fenistein, D.; Hecke, M. V. Kinematics: Wide shear zones in granular bulk flow. *Nature* **2003**, *425*, 256−256.
(2) Sundaresan, S. Some outstanding questions in handling of cohesionless particles. *Powder Technol.* **2001**, *115*, 2−7.
(3) Silbert, L. E.; Ertas, D.; Grest, G. S.; Halsey, T. C.; Levine, D.; Plimpton, S. J. Granular flow down an inclined plane: Bagnold scaling and rheology. *Phys. Rev. E* **2001**, *64*, 051302.
(4) Tardos, G. I.; McNamara, S.; Talu, I. Slow and intermediate flow of a frictional bulk powder in the couette geometry. *Powder Technol.* **2003**, *131*, 23−39.
(5) Campbell, C. S. Granular shear flows at the elastic limit. *J. Fluid Mech.* **2002**, *465*, 261−291.
(6) Aarons, L.; Sundaresan, S. Shear flow of assemblies of cohesive and non-cohesive granular materials. *Powder Technol.* **2006**, *169*, 10−21.
(7) Chialvo, S.; Sun, J.; Sundaresan, S. Bridging the rheology of granular flows in three regimes. *Phys. Rev. E* **2012**, *85*, 021305.
(8) Ji, S.; Shen, H. Internal parameters and regime map for soft polydispersed granular material. *J. Rheol.* **2008**, *52*, 87−103.
(9) Lun, C. K. K.; Savage, S. B.; Jeffrey, D. J.; Chepurniy, N. Kinetic theories for granular flow: Inelastic particles in couette flow and slightly inelastic particles in general flowfield. *J. Fluid Mech.* **1984**, *140*, 223−256.
(10) Jenkins, J. T.; Savage, S. B. A theory for the rapid flow of identical, smooth, nearly elastic, spherical particles. *J. Fluid Mech.* **1983**, *130*, 187−202.
(11) Jenkins, J. T.; Richman, M. W. Kinetic theory for plane shear flows of a dense gas of identical, rough, inelastic, circular disks. *Phys. Fluids* **1985**, *28*, 3485−3494.
(12) Schaeffer, D. G. Instability in the evolution equations describing incompressible granular flow. *J. Differential Equations* **1987**, *66*, 19−50.
(13) Nedderman, R. M. *Statics and Kinematics of Granular Materials*, 2nd ed.; Cambridge University Press: Cambridge, U.K., 1992.
(14) Sun, J.; Sundaresan, S. A constitutive model with microstructure evolution for flow of rate-independent granular materials. *J. Fluid Mech.* **2011**, *682*, 590−616.
(15) MiDi, G. D. R. On dense granular flows. *Eur. Phys. J. E* **2004**, *14*, 341−365.
(16) Vidyapati, V.; Langroudi, M. K.; Sun, J.; Sundaresan, S.; Tardos, G. I.; Subramaniam, S. Experimental and computational studies of dense granular flow: Transition from quasi-static to intermediate regime in a couette shear device. *Powder Technol.* **2012**, *220*, 7−14.
(17) Benyahia, S. Validation study of two continuum granular frictional flow theories. *Ind. Eng. Chem. Res.* **2008**, *47*, 8926−8932.
(18) Beverloo, W. A.; Leniger, H. A.; Velde, J. The flow of granular solids through orifices. *Chem. Eng. Sci.* **1961**, *15*, 243−250.
(19) Syamlal, M.; Rogers, W.; O'Brien, T. J. Mfix documentation: Theory guide; Technical Report DOE/METC-95/1013, NTIS/DE95000031. National Energy Technology Laboratory, Department of Energy, 1993. See also URL http://www.mfix.org.
(20) Srivastava, A.; Sundaresan, S. Analysis of a frictional−kinetic model for gas−particle flow. *Powder Technol.* **2003**, *129*, 72−85.
(21) Nedderman, R. M.; Tuzun, U.; Savage, S. B.; Houlsby, G. T. The flow of granular materials I: Discharge rate from hoppers. *Chem. Eng. Sci.* **1982**, *37*, 1597−1609.
(22) Landry, J. W.; Gary, S. G.; Plimpton, S. J. Discrete element simulations of stress distribution in silos: Crossover from two to three dimensions. *Powder Technol.* **2004**, *139*, 233−239.
(23) Goda, T. J.; Ebert, F. Three-dimensional discrete element simulations in hoppers and silos. *Powder Technol.* **2005**, *158*, 58−68.
(24) Ketterhagen, W. R.; Jennifer, C. S.; Wassgren, C. R.; Hancock, B. C. Predicting the flow mode from hoppers using the discrete element method. *Powder Technol.* **2009**, *195*, 1−10.
(25) Engblom, N.; Saxen, H.; Zevenhoven, R.; Nylander, H.; Enstad, G. G.; Murtomma, M. Effect of material properties on segregation of binary and ternary powder mixtures in a small scale cylindrical silo. *Ind. Eng. Chem. Res.* **2011**, *50*, 11097−11108.
(26) Vidyapati, V.; Subramaniam, S. Granular rheology and phase transition: DEM simulations and order parameter based constitutive model. *Chem. Eng. Sci.* **2012**, *72*, 20−34.
(27) Anand, A.; Curtis, J. S.; Wassgren, C. R.; Hancock, B. C.; Ketterhagen, W. R. Predicting discharge dynamics from a rectangular hopper using the discrete element method (DEM). *Chem. Eng. Sci.* **2008**, *63*, 5821−5830.
(28) Brown, R. L.; Richards, J. C. Profile of flow of granules through apertures. *Trans. Inst. Chem. Eng.* **1960**, *38*, 260−269.
(29) Ristow, G. H. Outflow rate and wall stress for two-dimensional hoppers. *Physica A* **1997**, *235*, 319−326.
(30) Bagnold, R. A. Experiments on a gravity-free dispersion of large solid spheres in a Newtonian fluid under shear. *Proc. R. Soc. London, Ser. A* **1954**, *225*, 49−63.
(31) Johnson, P. C.; Jackson, R. Frictional−collisional constitutive relations for granular materials, with application to plane shearing. *J. Fluid Mech.* **1987**, *176*, 67−98.
(32) Savage, S. B Analyses of slow high-concentration flows of granular materials. *J. Fluid Mech.* **1998**, *377*, 1−26.
(33) Evans, D. J.; Morriss, G. P. *Statistical Mechanics of Non-equillibrium Liquids*, 2nd ed.; Academia Press: New York, 1990.
(34) Lees, A.; Edwards, S. The computer study of transport process under extreme conditions. *J. Phys. C: Solid State Phys.* **1972**, *5*, 1921−1929.